Acta Biomaterialia 188 (2024) 212–222

Contents lists available at ScienceDirect

Acta Biomaterialia

journal homepage: www.elsevier.com/locate/actbio

Full length article

Latent stem cell-stimulating radially aligned electrospun nanofibrous patches for chronic tympanic membrane perforation therapy

Juo Lee[a,b,1], Sangbae Park[c,d,e,1], Beomyong Shin[f,1], Yeon Ju Kim[g,h], Sungmin Lee[i], Jungsil Kim[j], Kyoung-Je Jang[k,l], Oak-Sung Choo[g], Jangho Kim[m,n,o], Hoon Seonwoo[b,p,*], Jong Hoon Chung[e,q,*], Yun-Hoon Choung[g,*]

[a] Department of Animal Science & Technology, Sunchon National University, Suncheon, 57922, Republic of Korea
[b] Interdisciplinary Program in IT-Bio Convergence System, Sunchon National University, Suncheon, 57922, Republic of Korea
[c] Department of Biosystems Engineering, Seoul National University, Seoul 08826, Republic of Korea
[d] Integrated Major in Global Smart Farm, College of Agriculture and Life Sciences, Seoul National University, Seoul 08826, Republic of Korea
[e] Research Institute for Agriculture and Life Sciences, Seoul National University, Seoul, 08826, Republic of Korea
[f] Department of Biomedical Sciences, BK21 Plus Research Center for Biomedical Sciences, Ajou University Graduate School of Medicine, Suwon, 16499, Republic of Korea
[g] Department of Otolaryngology, Ajou University School of Medicine, Suwon, 16499, Republic of Korea
[h] Department of Neurology, Yonsei University College of Medicine, Seoul, Republic of Korea
[i] Department of Human Harmonized Robotics, College of Engineering, Sunchon National University, Suncheon 57922, Republic of Korea
[j] Department of Smart Bio-Industrial Mechanical Engineering, College of Agriculture and Life Sciences, Kyungpook National University, Daegu 41566, Republic of Korea
[k] Department of Bio-Systems Engineering, Institute of Smart Farm, Gyeongsang National University, Jinju, 52828, Republic of Korea
[l] Institute of Agriculture & Life Science, Gyeongsang National University, Jinju, 52828, Republic of Korea
[m] Department of Convergence Biosystems Engineering, Chonnam National University, Gwangju, 61186, Republic of Korea
[n] Department of Rural and Biosystems Engineering, Chonnam National University, Gwangju, 61186, Republic of Korea
[o] Interdisciplinary Program in IT-Bio Convergence System, Chonnam National University, Gwangju, 61186, Republic of Korea
[p] Department of Convergent Biosystems Engineering, College of Life Science and Natural Resources, Sunchon National University, Suncheon, 57922, Republic of Korea
[q] ELBIO Inc, Seoul 08812, Republic of Korea

ARTICLE INFO

Article history:
Received 20 December 2023
Revised 12 September 2024
Accepted 12 September 2024
Available online 18 September 2024

Keywords:
Chronic otitis media
Tympanic membrane
Radial alignment
Stem cell stimulating therapy
Insulin-like growth factor-binding protein 2
Nanofibers

ABSTRACT

Chronic tympanic membrane (TM) perforation is a tubotympanic disease caused by either traumatic injury or inflammation. A recent study demonstrated significant progress in promoting the regeneration of chronic TM perforations through the application of nanofibers with radially aligned nanostructures and controlled release of growth factors. However, radially aligned nanostructures with stem cell-stimulating factors have never been used. In this study, insulin-like growth factor binding factor 2 (IGFBP2)-incorporated radially aligned nanofibrous patches (IRA-NFPs) were developed and applied to regenerate chronic TM perforations. The IRA-NFPs were prepared by electrospinning 8 wt% polycaprolactone in trifluoroethanol and acetic acid (9:1). Random nanofibers (RFs) and aligned nanofibers (AFs) were successfully fabricated using a flat plate and a custom-designed circular collector, respectively. The presence of IGFBP2 was confirmed via Fourier transform infrared spectroscopy and the release of IGFBP2 was sustained for up to 20 days. *In vitro* studies revealed enhanced cellular proliferation and migration on AFs compared to RFs, and the incorporation of IGFBP2 further promoted these effects. Quantitative real-time PCR revealed mRNA downregulation, correlating with accelerated migration and increased cell confluency. *In vivo* studies showed IGFBP2-loaded RF and AF patches increased regeneration success rates by 1.59-fold and 2.23-fold, respectively, while also reducing healing time by 2.5-fold compared to the control. Furthermore, IGFBP2-incorporated AFs demonstrated superior efficacy in healing larger perforations with enhanced histological similarity to native TMs. This study, combining stem cell stimulating factors and aligned nanostructures, proposes a novel approach potentially replacing conventional surgical methods for chronic TM perforation regeneration.

* Corresponding authors.
E-mail addresses: uhun906@scnu.ac.kr (H. Seonwoo), jchung@snu.ac.kr (J.H. Chung), yhc@ajou.ac.kr (Y.-H. Choung).
[1] These authors contribute to the study equally.

https://doi.org/10.1016/j.actbio.2024.09.019

Statement of significance

Chronic otitis media (COM) affects approximately 200 million people worldwide due to inflammation, inadequate blood supply, and lack of growth factors. Current surgical treatments have limitations like high costs and anesthetic risks. Recent research explored the use of nanofibers with radially aligned nanostructures and controlled release of growth factors to treat chronic tympanic membrane (TM) perforations. In this study, insulin-like growth factor binding protein 2 (IGFBP2)-incorporated radially aligned nanofibrous patches (IRA-NFPs) were developed and applied to regenerate chronic TM perforations. We assessed their properties and efficacy through *in vitro* and *in vivo* studies. IRA-NFPs showed promising healing capabilities with chronic TM perforation models. This innovative approach has the potential to improve COM management, reduce surgery costs, and enhance patient safety.

1. Introduction

Chronic otitis media (COM) affects nearly 200 million people worldwide and is associated with infection of the mucosal lining of the middle ear cleft [1]. The COM is typically attributed to the chronic perforation of tympanic membrane (TM) [1-3]. Due to inflammation, lack of blood supply and lack of growth factors, the chronic TM perforations do not regenerate well [4], which is why the regeneration of the chronic TM perforation is very important for the COM therapy [5,6]. Despite surgical methods such as myringoplasty and tympanoplasty boasting success rates exceeding 80 % [7], their efficacy is hindered by significant challenges including the inherent risks linked to anesthesia, considerable expenses, and requirements for additional surgeries to address donor site issues. These obstacles present major challenges for the management of COM [8,9]. Nonsurgical methods with simpler but highly successful outcomes would be good alternatives to lower huddles for patient safety and cost-effectiveness [10,11]. To this end, growth factors, *e.g.*, epidermal growth factor (EGF) [1,12-14], heparin-binding epidermal growth factor-like growth factor (HB-EGF) [15], insulin-like growth factor (IGF) [16], platelet-derived growth factor (PDGF) [8], and fibroblast growth factor (FGF) [5,9] have been used to enhance proliferation and migration of adjacent TM tissues. Applications of various biomaterials including silk, collagen, alginate, chitosan, and synthetic polymers in the TM perforation treatment has been under consideration [7,11,17-20]. A remarkable example is bacterial cellulose (BC), which has appropriate properties such as water retention, elasticity, mechanical strength, thermal stability, and transparency for application in TM regeneration [21]. The combination of biomaterials and growth factors is also a good strategy [3,4,22,23]. Recently, nanostructures have been reported to regulate cellular functions and tissue regeneration [24]. Nanotopography promotes the cellular migration, adhesion, and differentiation of hMSCs [25]. The nanostructures are also applicable in the regeneration of TM. A nanofibrous patch based on BC and chitin nanofibrils (CNs) exhibited successful growth, improved indirect antimicrobial activity, and upregulation of mRNA expression related to TM perforation healing, as it was tested *in vitro* using human dermal keratinocytes and human umbilical vein endothelial cells, which are model cells for TM [26]. Furthermore, radially aligned nanofibrous patches demonstrate positive effects on cellular migration and proliferation. Human dural fibroblasts cultured on radially aligned fibers exhibited an elongated shape with enhanced directional migration toward the center of the scaffolds [27]. The radially aligned nanofibrous patches releasing EGF (ERA-NFPs) have been reported to show excellent results in treating chronic TM perforation [12]. Owing to the synergic effects of their nanostructure and capacity for EGF release, ERA-NFPs exhibited the highest rate of TM regeneration with enhanced similarity to native TMs. Therefore, the use of nanostructures with various types of growth factors may be a straightforward method for the chronic TM regeneration.

Stem cells have been used in many areas of regenerative medicine [6,22,28,29]. They have been widely used for scar healing including skin wounds, which have similar structures to the TM [30]. The stem cells not only develop new tissues, but also secrete several proteins related to trophic factor [31], extracellular matrix formation [32], neovascularization [33], and immunity [34], resulting in the restoration of physiological balance. In aged tissues such as chronic TM perforation, a lack of neovascularization [35-38], trophic and matrix-related factors, and an increase in inflammatory cells [39] hinder complete tissue healing. These elements are intricately related to the reduction in populations of stem cells, that is, the influence of stem cells was greatly reduced in chronic TM perforations [28,30]. The implementation of latent stem cells as a potential strategy holds promise, given the vulnerability of transplanted stem cells to dehydration, which may substantially compromise their viability [22,23]. Our group has shown that latent stem cells are present in all three layers of the TM [17], but most latent epithelial progenitors located near the handle of malleus. However, damage to the structure severely reduced stem cell populations, resulting in irreversible chronic suppurative otitis media [14,34,37]. In order to reestablish the guidance of dormant stem cells in the process of regenerating chronic TM perforations, the utilization of insulin-like growth factor binding protein 2 (IGFBP2) has been suggested. IGFBP2 is recognized for its role in binding to and regulating the effects of insulin-like growth factor (IGF) [40], thereby serving as a potential stimulant for dormant stem cells [41]. In our previous study, we developed and utilized chitosan patch scaffolds (IGFBP-CPSs) containing IGFBP2 to facilitate the regeneration of chronic TM perforations through the activation of latent skin stem cells. The result showed that IGFBP2-incorporated chitosan patch scaffolds successfully regenerated TM with substantial histological similarity to the intact tissues and exhibited a higher success rate compared to the spontaneous healing (SH) group, exhibiting they were effective in regenerating chronic TM perforations compared to cytokine-free chitosan patch scaffolds [22]. However, the simultaneous use of IGFBP2 and radially aligned nanostructure for the regeneration of chronic TM perforation has not been reported. We thus hypothesized that radially aligned electrospun nanofibrous patches incorporating IGFBP2 would demonstrate significant enhancement in the chronic TM perforation regeneration.

In this study, we developed IGFBP2-incorporated radially aligned nanofibrous patches (IRA-NFPs). This design represents a concurrent application of nanotopographical and stem cell-simulating biochemical cues, intending for the use in tissue-engineering applications aimed at the non-surgical healing of

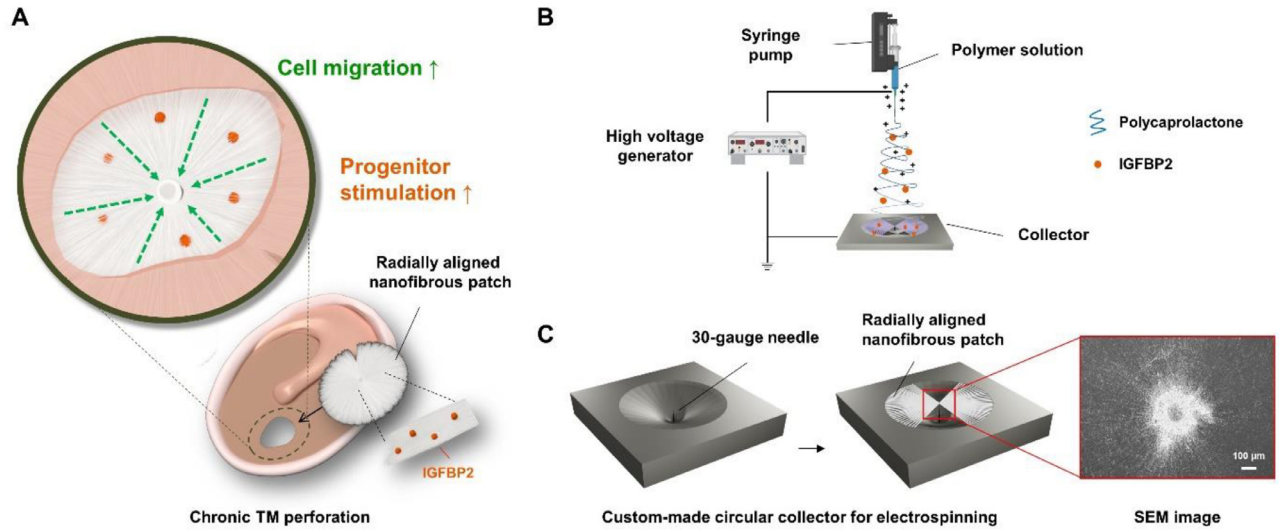

Fig. 1. Strategy of the study. (A) Schematic illustration of the strategy for regenerating chronic tympanic membrane (TM) perforations. Insulin-like growth factor-binding protein 2 (IGFBP2)-incorporated radially aligned nanofibrous patches (IRA-NFPs) were fabricated and used to regenerate chronic TM perforations. It was hypothesized that the radially oriented nanopatterns would promote cell migration and that IGFBP2 would be released from the patches to stimulate progenitor cells in the TM. (B) Schematic diagram of the electrospinning apparatus used to fabricate PCL patches containing IGFBP2 for TM regeneration. This apparatus generates electrically charged jets from a polymer solution containing PCL and IGFBP2. As the solvent evaporates and accumulates on the collector, a PCL nanofibrous structure is formed. (C) Electrospinning collector system for radially aligned fibers. The fibers form a radially aligned pattern extending outward from the central needle, guided by the unique electric field distribution within the central needle and the collector, which promotes radial alignment from the center.

chronic TM perforations (Fig. 1A). This study introduced the application of IGFBP2 as a stimulatory agent for stem cells and the implementation of nanostructures encompassing both radially aligned and randomly oriented nanofibers with the aim of fostering the regeneration of chronic TM perforations. First, IRA-NFPs were prepared and their morphological properties were evaluated. Next, *in vitro* release and cell viability assays were conducted, and the wound healing capability of IRA-NFPs was investigated. Quantitative real-time PCR (qRT-PCR) analysis was performed to investigate mRNA expression levels related to migration and cell responses. Finally, an *in vivo* study was performed using a chronic TM perforation animal model to evaluate the healing efficacy of the IRA-NFPs.

2. Materials and methods

2.1. Materials

IGFBP2 (R&D Systems Inc., Minneapolis, MN, USA), polycaprolactone (Mn: 80,000, Sigma-Aldrich, St. Louis, MO, USA), trifluoroethanol (Sigma-Aldrich, St. Louis, MO, USA), acetic acid (Duksan Co., Ltd, Seoul, South Korea), collagenase type I (0.05 %, Sigma-Aldrich, St. Louis, MO, USA), fetal bovine serum (Welgene Inc., Gyeongsan-si, South Korea), phosphate-buffered saline (Welgene Inc., Gyeongsan-si, South Korea), Dulbecco's modified Eagle's medium (Welgene Inc., Gyeongsan-si, South Korea), EZ-cytox Cell Viability Assay Kit (Daeillab Service Co., Ltd, Suwon-si, South Korea), Oris™ Cell Migration Assay Kit (AMSBIO, Abingdon, UK), Zoletil® 50 (Virvac Laboratories, Carros, France), Rompun® (2 %, Bayer Korea, Ansan-si, South Korea), mitomycin C (0.5 mg/mL, Kyowa, Tokyo, Japan), dexamethasone disodium phosphate (5 mg/mL, Ilsung, Seoul, South Korea), Tarivid® ophthalmic ointment (Santen Pharmaceutical Co., Ltd, Osaka, Japan), Calci-Clear Rapid HS-105 (National Diagnostics, Atlanta, GA, USA), hematoxylin (Youngdong Pharmaceutical Co., Seoul, South Korea) and eosin (Muto Pure Chemical Co., Tokyo, Japan) were used.

2.2. Fabrication of the IRA-NFPs

To produce IRA-NFPs, an electrospinning process was employed using an 8 wt% solution of polycaprolactone (PCL) in a mixture of trifluoroethanol and acetic acid at a volumetric ratio of 9:1 (Fig. 1B). The solution also contained a 0.2 μg/mL of IGFBP2, which was determined based on the optimal IGFBP2 concentration identified in our previous study [22]. In the electrospinning process, an applied voltage of 18 kV was maintained between the needle and the collector, while the solution's flow rate was configured at 0.3 ml/h. Additionally, a distance of 10 cm was upheld between the needle and the collector. Extrusion was carried out using a 22-gauge needle. Random nanofibers (RFs) were deposited onto a flat plate, while aligned nanofibers (AFs) were deposited onto a custom-made circular collector (Fig. 1C). The electrospinning process was conducted under static conditions, during which the collectors remained stationary. The experimental groups were categorized based on fiber alignments and the presence of IGFBP2: random fibers without IGFBP2 (RF-w/oIGFBP2), aligned fibers without IGFBP2 (AF-w/oIGFBP2), random fibers with IGFBP2 (RF-w/IGFBP2), and aligned fibers with IGFBP2 (AF-w/IGFBP2).

2.3. Characterizaiton of the IRA-NFPs

The external morphologies of the patches were examined utilizing a field emission scanning electron microscopy (FESEM) system (JSM-5410LV; JEOL, Tokyo, Japan) operating at an acceleration voltage of 2 kV. Subsequently, the orientation and coherence of nanofibers (NFs) were quantified utilizing the ImageJ software (Fig. S1). Specifically, we employed the OrientationJ plugin to analyze the nanofibers from FESEM images. A 3 × 3 grid system was used to select eight Regions of Interest (ROIs) around a central empty grid, enabling systematic analysis of fiber architecture. Fiber orientations were mapped in relation to circumferential and axial directions to quantify radial alignment patterns. An orientation map provided a visual representation of fiber directional trends, while a coherency map assessed fiber alignment and structural organization. The analysis concluded with a Hue-Saturation-Brightness

(HSB) color-coded map, where hue denotes local fiber orientation, saturation indicates coherency levels, and brightness represents original FESEM image intensity. A histogram of local orientations was also constructed to quantify the distribution of fiber angles.

The Fourier Transform Infrared spectroscopy (FT-IR) was conducted to validate the existence of the N–H band associated with the integrated IGFBP2. Infrared spectra in the transmission mode were acquired within the wavenumber interval of 4000 to 650 cm^{-1}, employing an FT-IR spectrometer (Nicolet 6700, Thermo Scientific, USA) with a resolution of 8 cm^{-1}. The release of IGFBP2 was analyzed by a soaking assay. The patches were positioned within the wells of a 96-well plate, accompanied by the addition of 1 mL of phosphate-buffered saline (PBS) in each well. The 96-well plate was maintained at a temperature of 36.5 °C. Subsequently, at the designated time intervals, the samples were retrieved, and each well was replenished with 1 mL of fresh PBS. The IGFBP2 in each collected sample was accomplished through an enzyme-linked immunosorbent assay (ELISA). The static water contact angles of both the radially aligned and random PCL patches were evaluated using the sessile drop technique at ambient temperature. A contact angle meter (Easy-Drop, Kruss, Hamburg, Germany) was utilized for this analysis. The static water contact angle was assessed on five distinct electrospun patch samples, and the mean value of water droplets (9.7 μm) was determined.

2.4. Mechanical testing of IRA-NFPs

To measure the mechanical properties of the TM patch, the puncture test was performed at a constant displacement rate of 0.2 mm/s (Fig. 3A) while recording load and displacement [adapted from 42]. The maximum load, displacement of the probe from initial contact to puncture of the patch, and area under the load-displacement curve were determined using a custom-written Matlab code, and the puncture strength, elongation to puncture, and energy to puncture were calculated. Puncture strength is calculated by:

$$Puncture\ strength\ (MPa) = \frac{F}{A_{cs}} \tag{1}$$

here F is the load required to puncture the patches and A_{cs} is the cross-sectional area of the edge of patches located in the path of the cylindrical opening of the patch holder. Elongation to puncture is calculated by:

$$Elongation\ to\ puncture\ (\%) = \frac{\sqrt{R^2 + D^2} - R}{R} \times 100 \tag{2}$$

where R is the radius of the patches exposed in the cylindrical opening of the patch holder (3 mm), and D is the displacement of the probe from the point of contact to the point of patch puncture. Elongation to puncture represents the change in radius from the pre-deformed state of the patch to the point of puncture. The stored energy required to puncture is calculated from the area under the load-displacement curve. It is normalized by a volume term to account for differences in patch thickness. Hence,

$$Energy\ to\ puncturep\ er\ unit\ volume(mJ/mm^3) = \frac{AUC}{V_c} \tag{3}$$

where V_c is the volume of the patch located in the opening of the patch holder.

2.5. In vitro studies

TM cells were extracted from 4-week-old female Sprague-Dawley rats. The TMs were aseptically excised from female Sprague-Dawley rats and finely minced using scissors. The TMs were subjected to three washes using a mixture of phosphate-buffered saline (PBS) and 0.05 % collagenase type I at a temperature of 37 °C for a duration of 30 min. Following the washes, the solution was neutralized using Dulbecco's modified Eagle's medium (DMEM) with low glucose content supplemented with 10 % fetal bovine serum (FBS). Subsequently, the neutralized solution was filtered through a 10-μm nylon mesh to obtain the desired outcome. After centrifugation at 300 g for 3 min, the fraction with a high cell density was obtained. This pellet was then resuspended in DMEM and cultured in basal media (DMEM, 10 % FBS, 1 % antibiotic/antimycotic) within a 37 °C incubator, supplemented with 5 % CO_2. The culture media were changed every 2 days prior to use. Cell viability was evaluated through WST-1 assay. The quantification of water-soluble formazan was performed using a multi-well spectrophotometer (Victor 3, Perkin Elmer, USA) by measuring its absorbance at 450 nm. The effect of the IRA-NFPs on the migration of TM cells was assessed with a Oris™ cell migration kit. Briefly, the IRA-NFPs were placed in the 96-well plate, and inserts were placed in the wells and aligned in a single direction. One hundred microliters of cell suspension containing 1×10^6 cells mL^{-1} was added to each well, and the plate was incubated at 37 °C overnight. The insert was then removed from each well. The wound sites were observed for one week or until the wounds were entirely closed, and the recovered areas were then measured using ImageJ software.

The effect of the IRA-NFPs on gene expression was evaluated by qRT-PCR analysis. The centrifuged cells were homogenized in TRIzol reagent, after which the total RNA was isolated according to the manufacturer's instructions. The RNA quality was checked using a Nanodrop 2000 spectrophotometer. The total RNA (1 μg) was then reverse-transcribed into complementary DNA (cDNA) using a SuperiorScript III cDNA Synthesis Kit. The cDNA was amplified with the following primers (Table 1): Col1a1, Col3a1, MMP3, Rac1, cadherin, VEGF, and MMP2. Relative gene expression was analyzed using the comparative threshold cycle method. The expression of the genes of interest was expressed as fold change relative to AF-wIGFBP2.

2.6. In vivo studies

A total of one hundred and twenty female Sprague-Dawley rats (8 weeks old, weighing 200–250 g) were employed for the present study. The surgical protocols were approved by the Institutional Animal Care and Use Committee (IACUC number, 2014-0069) of Ajou University School of Medicine, in compliance with the established principles for the ethical treatment and utilization of animals in experimental investigations. Diligent measures were taken to reduce the count of animals employed and to alleviate their discomfort. The approach for establishing the animal models with chronic TM perforation adhered to a precedent investigation [36]. Concisely, Sprague-Dawley rats were anesthetized using an intraperitoneal administration of Zoletil®50 and 2 % Rompun. The front section of the TM was mechanically perforated using a heated micropick, resulting in an approximately 50 % perforation size of the TM as observed under an operating microscope (Carl Zeiss, Jena, Germany). To avoid injury to the malleus handle and annulus, all perforations were made carefully during this procedure. Gel foam infused with 0.5 mg/mL mitomycin C was administered at the perforation site for a duration of 10 min. Subsequently, gel foam infused with 5 mg/mL dexamethasone disodium phosphate was applied to the perforation site for a period of 1 week. Following a week, a gel foam was extracted from the perforation site and subjected to an 8-week observation period. A total of one hundred and eight ears were included in this study, as ears with unsuitable conditions such as spontaneously healed ears, excessively large perforations, and ears from deceased rats were excluded from the analysis.

Table 1
Primer sequences for qRT-PCR.

Gene	Species	Forward	Reverse
Col1a1	Rat	GAGCGGAGAGTACTGGATCGA	CTGACCTGTCTCCATGTTGCA
Col3a1	Rat	TGCCATTGCTGGAGTTGGA	GAAGACATGATCTCCTCAGTGTTGA
Mmp3	Rat	CCACAGAATCCCCTGATGTC	CTGACTGCATCGAAGGACAA
Rac1	Rat	GCCGTTGGTAAAACCTGC	GGGACGCAGTCTGTCATA
E-cad	Rat	CAAATCCAACAGGGACAAAGA	GCGTCACTTTCAGCCAGCCTG
Vegf	Rat	GTACCTCCACCATGCCAAGT	AATAGCTGCGCTGGTAGACG
Mmp2	Rat	AAAGGAGGGCTGCATTGTGAA	CTGGGGAAGGACGTGAAGAGG
18s	Rat	GGTGCATGGCCGTTCTTA	TCGTTCGTTATCGGAATTAACC

To confirm the healing status of the patches, AF-w/IGFBP2 was applied to 37 ears, and RF-w/IGFBP2 was applied to 26 ears. Ears that healed spontaneously healing served as the control group (33 ears). Ofloxacin ointment was used to adhere the patches to the entire edge of the perforations. Weekly assessments were conducted on each ear utilizing an endoscopic camera over an 8-week period. The extent of perforation for each ear, expressed as a percentage (perforation area divided by pars tensa area, multiplied by 100 %), was quantified through the utilization of Image J software (National Institute of Health, USA). At the conclusion of the 8-week period, TM blebs were immobilized using 4 % paraformaldehyde and subsequently stored at 4 °C overnight. Following a 2-day decalcification process using Calci-Celar Rapid solution, certain specimens underwent staining utilizing hematoxylin and eosin. Bright field microscopy images were obtained using Picture Frame software (Olympus Optical, BX51, Tokyo, Japan).

2.7. Statistical analysis

Statistical analyses were performed suing the Statistical Package for the Social Sciences (SPSS) for Windows Ver. 12.0.1. For the purpose of comparing the means of distinct attributes associated with the growth factor-releasing nanofibrous patches, statistical analysis employed Duncan's least significant difference (LSD) approach and unpaired Student's *t*-tests. A significance level of $p < 0.05$ was established. To compare the healing rate means of TM perforations regenerated through IRA-NFPs and the control group, Chi-squared and Mann-Whitney tests were employed. The significance level was again set at $p < 0.05$.

3. Results

3.1. Characterization of the IRA-NFPs

The IRA-NFPs were successfully fabricated by the custom-made collectors [12]. A 30-gauge needle was chosen as the center of the collectors based on its effectiveness in gathering nanofibers with radial alignment and generating well-defined central regions. SEM images revealed that in the AFs, the nanofibers were well aligned toward the center, whereas the nanofibers of the RFs were randomly aligned without any tendency (Fig. 2A). Morphological analysis using FESEM revealed that nanofibers incorporated with IGFBP2 exhibited comparable fiber diameters to those composed of only PCL, with no statistically significant differences observed. The diameters of the nanofibers across all experimental groups were consistently <200 nm (Fig. 2B). Quantitative analysis using the ImageJ Orientation plugin revealed distinct differences in fiber alignment between the groups. The nanofibers in the RFs displayed a broad orientation distribution, whereas those in AFs exhibited a more narrowly oriented distribution (Fig. 2C). Correspondingly, the coherence of nanofibers in AFs was significantly higher than that in the RFs (Fig. 2D), indicating a more organized fiber structure in the AFs. The incorporation of IGFBP2 did not affect the orientation or coherence of AFs. Water contact angle analysis demonstrated that the AF-w/IGFBP2 group exhibited greater hydrophobicity compared to the RF-w/IGFBP2 group (Fig. 2E). FT-IR analysis of IGFBP2, as shown in Fig. 2F, revealed characteristic spectral features including specific peaks corresponding to C–N, N–H, and O=C–N bonds, providing confirmation of the structural integrity and presence of proteins in the sample. The release of IGFBP2 from the patches was measured by ELISA, showing continuous release over 20 days (Fig. 2G).

3.2. Mechanical properties of the IRA-NFPs

The mechanical properties of AFs and RFs were evaluated through uniaxial puncture tests. The results indicate that AFs have overall superior mechanical characteristics compared to RFs. Representative load-displacement curves of AFs and RFs, both approximately 350 μm in thickness, under quasi-static compressive loading are presented in Fig. 3B. Puncture strength analysis revealed that AFs were significantly stonger than RFs, with mean values of 0.86 ± 0.26 MPa and 0.18 ± 0.03 MPa, respectively (Fig. 3C). The elongation to puncture at failure was 51.0 ± 12.9 % for AFs and 20.3 ± 5.3 % for RFs (Fig. 3D). AFs demonstrated approximately 30 % greater elongation to puncture than RFs, indicating enhanced ductility and flexibility. The energy absorption capacity, calculated as energy to puncture per unit volume, was 0.44 ± 0.08 mJ/mm^3 for AF and 0.09 ± 0.01 mJ/mm^3 for RFs (Fig. 3E). AFs displayed an approximately 5-fold greater energy absorption capacity compared to RFs, demonstrating improved puncture resistance under loading conditions. This difference in the stored energy during deformation indicates distinct structural responses between two types of nanofibrous patches.

3.3. In vitro studies

Following the characterization of IRA-NFPs, their *in vitro* properties were evaluated. Initially, a wound-healing assay was conducted to assess the effect of IRA-NFPs on cellular migration. The assays demonstrated that wounds on AFs exhibited accelerated closure rates compared to those on RFs. By day 4, the AF-w/IGFBP2 group displayed significantly enhanced wound closure relative to other experimental groups (Fig. 4A and B). At day 7, no statistically significant differences were observed between the AF-w/IGFBP2 and RF-w/IGFBP2 groups. However, both IGFBP2-containing groups demonstrated significantly accelerated wound healing rates compared to other groups. Cell viability analysis revealed no significant differences among all samples on days 4 and 7 (Fig. 4C). However, on days 10 and 14, the cell viability of IRA-NFPs significantly increased compared to other groups. These results indicate that while cell viability does not significantly differ between AF and RF in terms of structural morphology, it is substantially influenced by IGFBP2. This suggests that IGFBP2 plays a more prominent role in determining cell viability than the structural differences between AF and RF.

Fig. 4D presents the qRT-PCR results for migration-related markers influenced by RF and AF, as well as cell response mark-

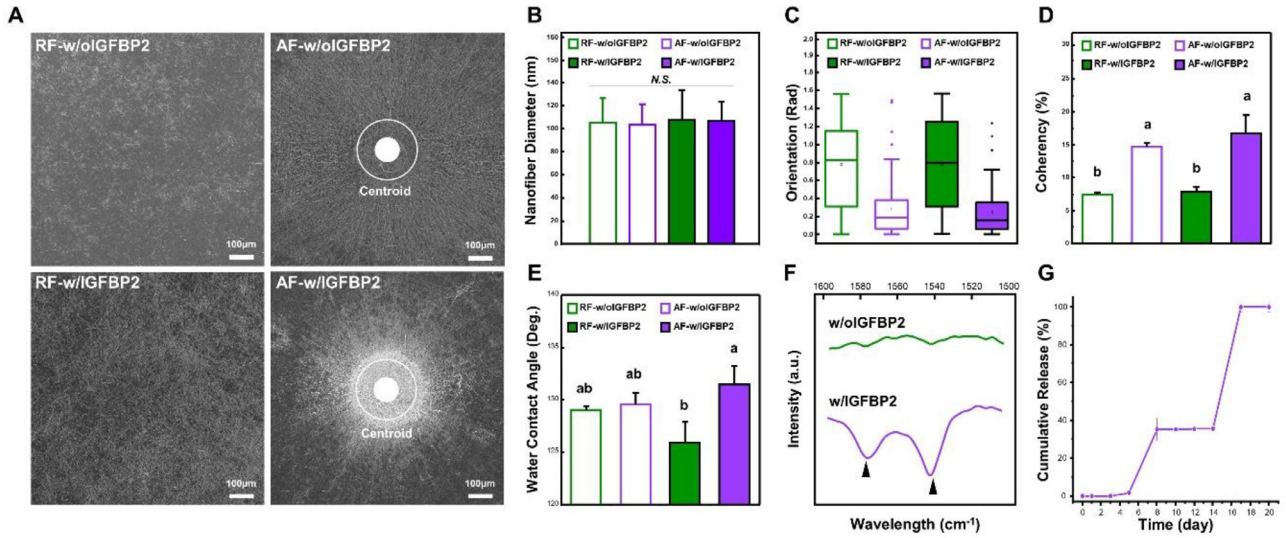

Fig. 2. Characteristics of IRA-NFPs. (A) Scanning electron microscopy (SEM) images of a random nanofiber (RF) patch and radially aligned nanofiber (AF) patches. The fibers in the AF patches are well aligned toward the centroid (Scale bar: 100 μm). (B) Quantitative analysis of nanofiber diameter among each group. There was no significant difference in nanofiber diameter between the groups. (C) Distributions of fiber orientation. Fibers from AF patches showed a highly ordered orientation to the centroid, whereas those from RF patches showed a wide range of orientation. (D) Coherence of nanofibers. Fibers from AF patches showed significantly higher coherence than those from RF patches. (E) Water contact angle analysis results. When IGFBP2 was incorporated, RF and AF showed a significant difference. In comparison, there was no significant difference between RF and AF when IGFBP2 is not incorporated. (F) Fourier transform infrared (FT-IR) spectra of nanofibers with and without IGFBP2. IGFBP2-loaded nanofibrous patches exhibited characteristic peaks in the N–H band (1540 and 1580 cm^{-1}). (G) Cumulative release profile of IRA-NFPs. The burst release of IGFBP2 observed twice: on day 5 and 14. Error bars in (B)-(E) and G represent the standard error of the mean. Duncan's multiple range test was used for D and E with $p < 0.05$. Results with the same letter indicate no statistical difference.

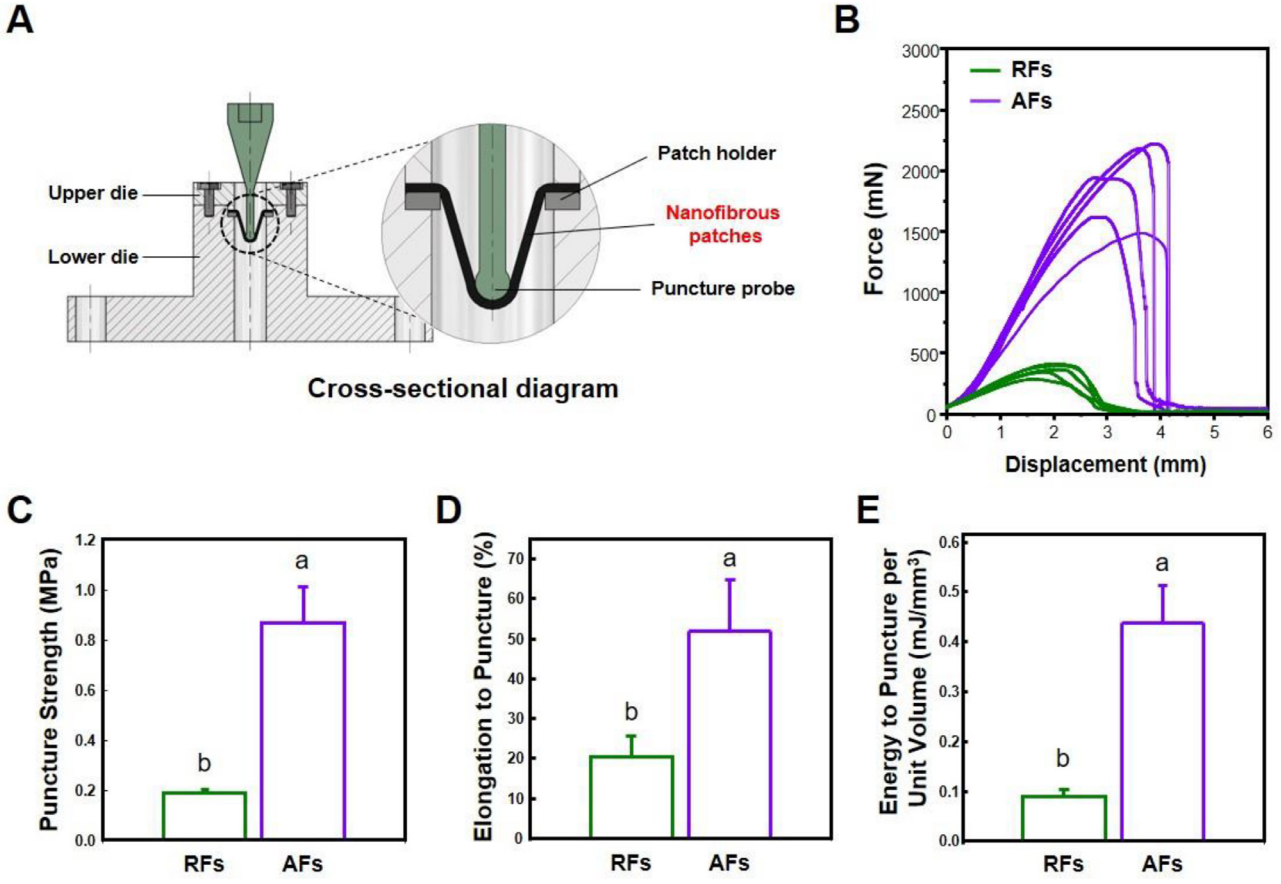

Fig. 3. Mechanical properties of IRA-NFPs. (A) Cross-sectional diagram of the puncture testing apparatus to measure the mechanical properties of nanofibrous patches. The puncture test was performed using a hemispherical probe (2 mm radius) at a displacement rate of 0.2 mm/s. (B) Load-displacement curves of random and aligned nanofibrous patches. Nanofibrous patches with AFs exhibited superior mechanical strength compared to those with RFs. (C) Puncture strength. Aligned nanofibrous patches demonstrated significantly higher resistance to puncture compared to random nanofibrous patches. (D) Elongation to puncture. The aligned nanofiber structure allowed for greater deformation before failure, indicating enhanced flexibility and durability. (E) Energy to puncture per unit volume of nanofibrous patches. AFs exhibited superior energy absorption capacity, suggesting improved resistance under mechanical loading. Error bars in (C)-(E) represent the standard error of the mean. The Student's *t*-test was used for statistical analysis in (C)-(E), with considered significance of $p < 0.05$. Results with the same letter indicate no statistical difference.

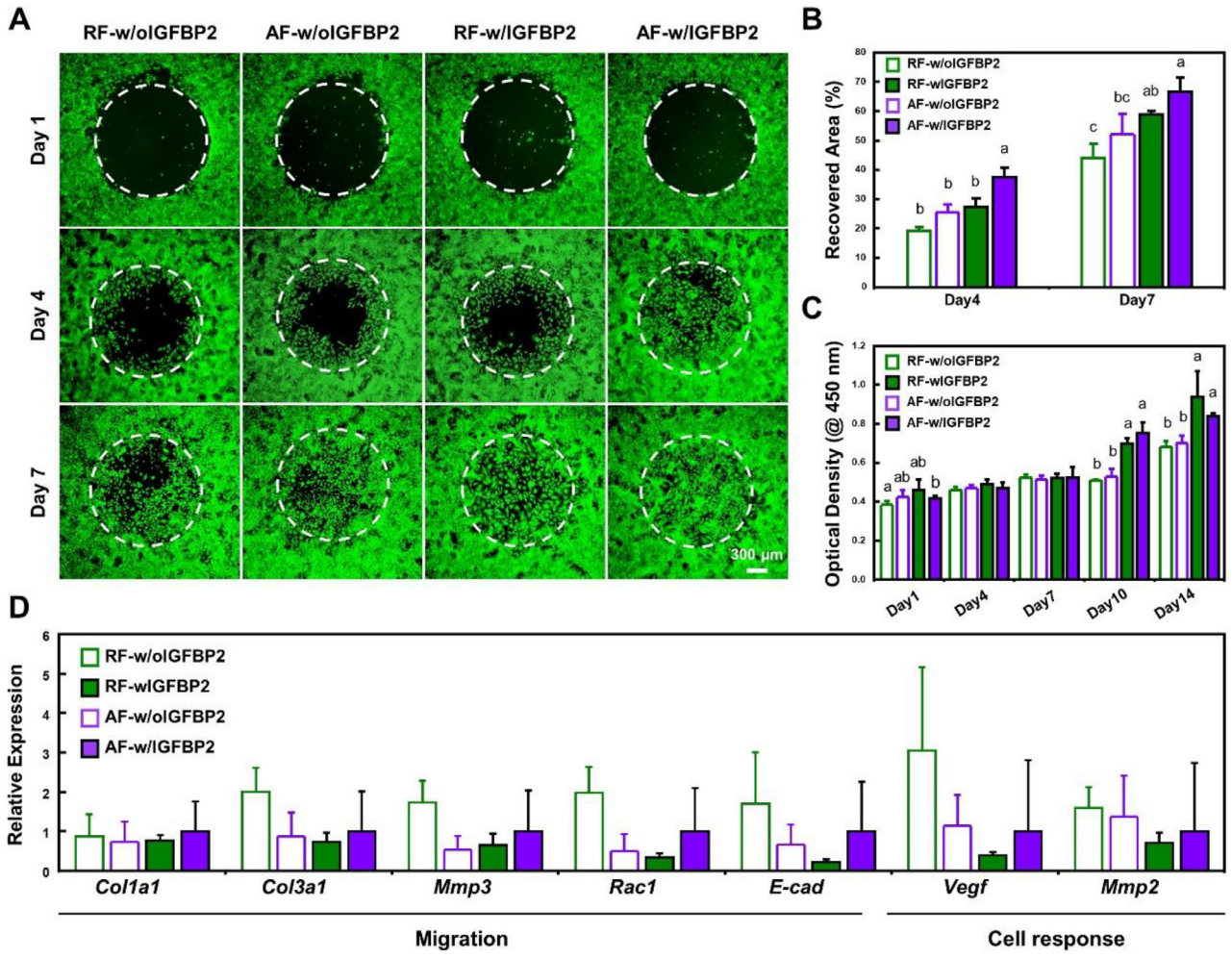

Fig. 4. *In vitro* study. (A) Wound-healing assay of IRA-NFPs for 7 days. AF-w/IGFBP2 exhibited the fastest wound-healing capability compared with other groups. Radial alignments and IGFBP2 release would interactively enhance the wound-healing capability of IRA-NFPs. (B) Recovery rate of IRA-NFPs. IGFBP2 and radially aligned nanostructures synergistically enhanced wound closure on day 4 and 7. (C) Cell viability result. The IRA-NFPs showed significantly higher cell metabolic activity than other groups. (D) The relative mRNA expressions related to migration and cell response. The IRA-NFPs showed decreased migration and cell response markers. Error bars in (B)-(D) represent standard errors of the mean. Statistical analysis was performed using Duncan's multiple range test for each group. Results with the same letter indicate no statistical difference.

ers associated with IGFBP2, obtained from cells cultured on IRA-NFPs for 7 days. Regarding the migration-related factors examined (*Col1a1, Col3a1, Mmp3, Rac1, Cadherin*), the RF-w/oIGFBP2 groups demonstrated decreased RNA expression levels in comparison to the AF-w/oIGFBP2 groups. This reduction is attributed to the majority of migration processes having already completed in these samples. Additionally, diminished expression of IGFBP2-related cell response factors (*Vegf, Mmp2*) was observed in the AF-w/IGFBP2 groups compared to the RF-w/IGFBP2 groups. This finding indicates that the AF-w/IGFBP2 groups may have reached a state of cell confluency induced by IGFBP2, leading to a subsequent decrease in RNA expression levels.

3.4. In vivo *studies*

In order to validate the effectiveness of IRA-NFPs, chronic TM perforation models were established and subsequently assessed for their regenerative potential. (Fig. S2). For this purpose, Choung's COM1 model developed by our group was applied to regenerate chronic TM perforations [7]. Chronic TM perforations were gently created by micropick along with mitomycin C and dexamethasone. After 8 weeks of observation, chronic perforation models were confirmed to be well maintained on rat TMs for at least 8 weeks (Fig. S2B). Before patch application, the size of the perforations was compared, and there was no significant difference among all groups (Fig. S2C). Therefore, the animal model of chronic TM perforation could be used to study without experimental bias. The efficacy of IGFBP2 was confirmed in a previous study, so IGFBP2-incorporated nanofibrous patches, which were RF-w/IGFBP2 and AF-w/IGFBP2, were used in this study and compared with the SH group. The closure rate of chronic TM perforation was observed at 8 weeks (Fig. 5A). The regeneration success rates of RF-w/IGFBP2 and AF-w/IGFBP2 were higher than the SH group; 19.2 % of RF-w/IGFBP2 group, 27.0 % of AF-w/IGFBP2 group, and 12.1 % of the SH group (Fig. 5B). When comparing the individual healing cases, AF-w/IGFBP2 was shown to heal larger perforations compared to RF-w/IGFBP2 (Fig. 5C, D, and E). Histologically, the TMs healed by AF-w/IGFBP2 showed similar thickness to normal TMs (Fig. 6A and B). The closure rate of the AF-w/IGFBP2 group was higher than that of the RF-w/IGFBP2 group, but there was no significant difference between the RF-w/IGFBP2 and AF-w/IGFBP2 groups. The healing time of IRA-NFPs was approximately 2.5 times faster than that of SH group (Fig. 6C). The closure area of TM perforations was reduced by approximately 20 % by both patches, but untreated TM perforations were conversely increased compared to the initial size of chronic TM perforations (Fig. 6D). Perforation size was

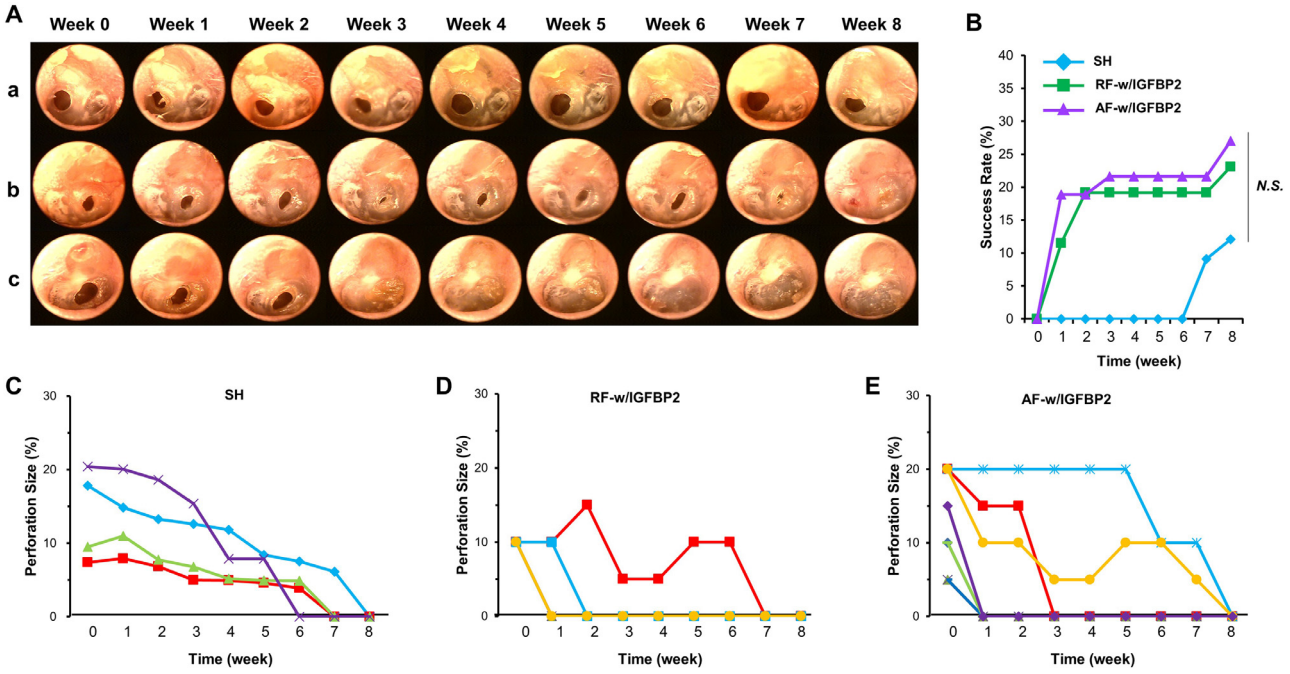

Fig. 5. *In vivo study.* (A) Serial images of chronic TM perforations: (a) unhealed chronic TM perforation, (b) healed chronic TM perforation with RF-w/IGFBP2, and (c) healed chronic TM perforation with AF-w/IGFBP2. (B) Healing rate of each group. All groups were not significant by Mann-Whitney U test. (C)-(E) Continuous changes in perforation size for healing cases. (C) Spontaneous healing (SH) cases, (D) RF-w/IGFBP2 group cases, and (E) AF-w/IGFBP2 cases. Cases of AF-w/IGFBP2 showed a faster healing rate and a faster healing response than other groups.

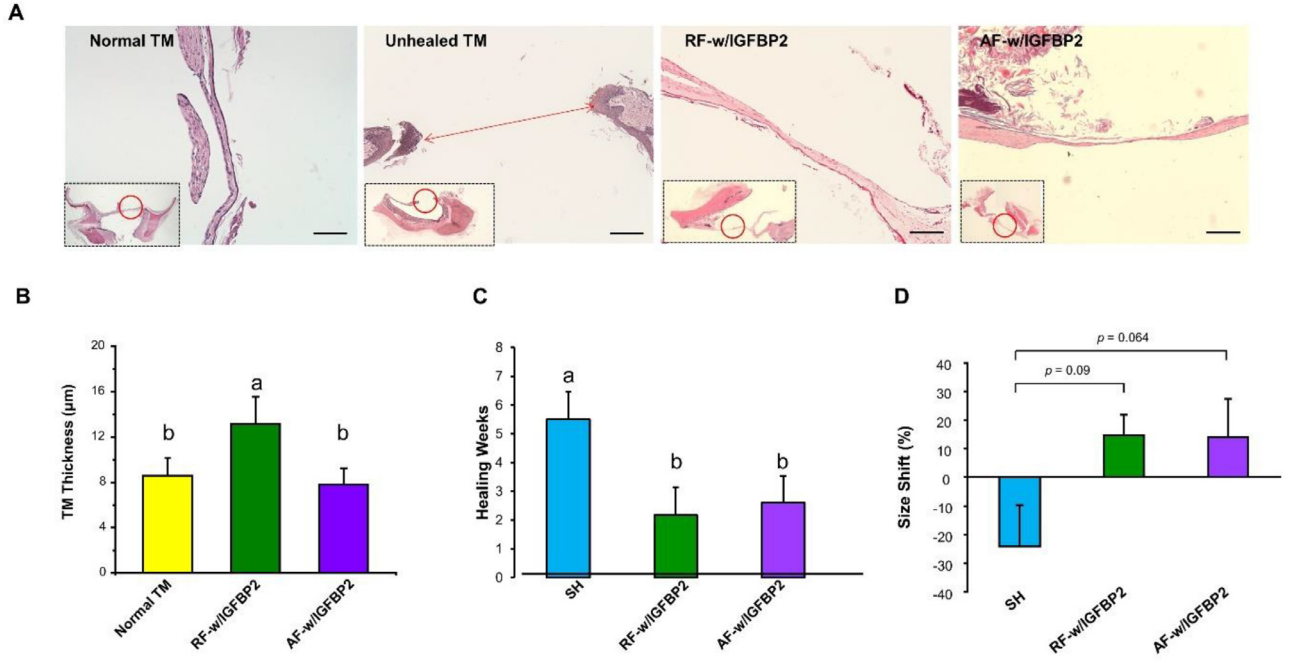

Fig. 6. Regeneration of chronic TM perforation. (A) Histologic analysis. Normal TM, unhealed chronic TM perforation with SH, healed chronic TM perforation with RF-w/IGFBP2, and healed chronic TM perforation with AF-w/IGFBP2 were shown. The AF-w/IGFBP2 group showed morphologic features similar to normal TM (scale bars = 50 μm). (B) Mean thickness of TMs. The AF-w/IGFBP2 group had almost the same thickness as the normal TM group. (C) Healing time of each group. The healing time for RF-w/IGFBP2 and AF-w/IGFBP2 was significantly reduced compared to that of SH. (D) Perforation size shift according to initial perforation size. The AF-w/IGFBP2 group showed an almost significant difference. Error bars in (B)-(D) represent the standard error of the mean. Statistical analysis was performed using Mann-Whitney U tests for each group, with considered significance of $p < 0.05$. Results with the same letter indicate no statistical difference.

14.60 ± 8.87 %, 13.92 ± 18.02 %, and −22.41 ± 14.87 % compared to 1 week in the RF-w/IGFBP2, AF-w/IGFBP2, and SH groups, respectively (Figs. S3, S4, and S5).

4. Discussion

The successful fabrication of IRA-NFPs using custom-made collectors demonstrates the efficacy of this approach in producing nanofibers with radial alignment and well-defined central regions. The radially aligned nanostructure plays a crucial role in maintaining the desired properties of IRA-NFPs. In the water contact angle analysis, the AF-w/IGFBP2 group exhibited a more hydrophobic characteristics compared to the RF-w/IGFBP2 group. Previous studies have reported increased hydrophobicity in aligned fibers [43,44]. This effect is likely due to the energy barriers introduced by the aligned surfaces, which limit droplet elongation and result in higher contact angles. The sustained release of IGFBP2 over 20 days suggests the potential for prolonged therapeutic effects *in vivo*. However, the release characteristics of IRA-NFPs were reduced compared to previous studies using EGF, possibly due to the molecular characteristics of IGFBP2 and its interactions with PCL. The relatively larger molecular weight of IGFBP2 (∼35 kDa) compared to EGF (∼6 kDa) may have caused it to become physically trapped within the polymer network, delaying its release [45,46]. Additionally, the interaction between IGFBP2 and PCL leads to stronger adherence to the polymer network [47,48]. As the polymer chains gradually degrade, these entrapped molecules are suddenly released in bursts. In addition, the radially aligned nanofibrous structure of the developed IRA-NFPs offers superior mechanical advantages compared to RFs. The enhanced mechanical strength of the AFs can be attributed to the directional alignment of the nanofibers within the patches, allowing for efficient load distribution across the entire patch. This may provide additional benefits in withstanding the physiological stresses experienced by the tympanic membrane. Furthermore, the increased capacity for energy absorption of AFs also suggests improved puncture resistance. In contrast, the random fiber orientation in the RFs resulted in a non-uniform stress distribution, which may lead to the formation of localized weak points. It also contributes to their lower maximum strength and increased ductility. Notably, both AFs and RFs exhibited mechanical strength that surpassed the typical pressure experienced by the human tympanic membrane during daily activities, which ranged from approximately 10^{-5} to 10^{2} mJ/mm^3 [49].

In vitro studies demonstrated a synergistic effect between the radially aligned nanostructure and IGFBP2 on TM cells, highlighting the potential for enhanced IGFBP2 efficacy when presented within an appropriate nanostructured environment. Notably, the effect of radial alignments on migration appeared to be more pronounced than that of IGFBP2 alone, suggesting that topographical guidance may play a crucial role in directing cellular behavior [12]. This observation aligns with the principle that cellular orientations tend to follow the alignment of nanofibers in the scaffold. The synergistic effect of AFs and IGFBP2 on TM cells emphasizes the necessity of integrating both biochemical and structural cues in scaffold design for tissue engineering applications. Our analysis of migration-related factors (*Col1a1, Col3a1, Mmp3, RaC1, Cadherin*) revealed lower RNA expression levels in the RF-w/oIGFBP2 groups compared to the AF-w/oIGFBP2 groups. This pattern suggests that by day 7, cellular migration in the AFs had substantially progressed, leading to a downregulation of these factors. In contrast, migration appeared to be ongoing in the RFs. Additionally, we noted reduced expression of IGFBP2-related cell response factors (*Vegf, Mmp2*) in the AF-w/IGFBP2 groups relative to the RF-w/IGFBP2 groups, indicating that the AF-w/IGFBP2 groups likely achieved IGFBP2-induced cell confluency earlier, resulting in a subsequent decline in RNA expression levels. These gene expression patterns collectively support the hypothesis that aligned fibers promote more rapid migration and cell confluency compared to randomly oriented fibers, an effect that is particularly pronounced in the presence of IGFBP2. This finding highlights a synergistic interaction between nanofiber alignment and biochemical factor, suggesting a promising approach to guide and enhance cellular responses. This approach could potentially improve treatments for tympanic membrane perforations.

The results of surgical methods, tympanoplasty or myringoplasty, were reported to have the highest success rates in the clinic [2,50]. In the *in vivo* studies, Choung's COM model 1 was used as a chronic TM perforation model, with its stability already validated in several studies [7,12,22,23,51]. The results showed that almost 30 % of chronic TM perforations were regenerated by AF-w/IGFBP2 (Table 2). Although the success rate did not reach statistical significance among the experimental groups, AF-w/IGFBP2 demonstrated a superior capability in treating larger perforations and resulted in histologically improved similarity to normal TM. Additionally, the AF-w/IGFBP2 showed accelerated healing rates, even for larger perforations. This acceleration in healing speed, regardless of initial perforation size, suggests that our platform does exhibit a degree of efficacy in the chronic TM perforation models. While the healing success rates of IRA-NFPs are not as high as those achieved through surgical methods, this therapeutic approach presents a promising alternative for patients. In recent years, numerous studies have explored the use of growth factors for the treatment of chronic tympanic membrane perforation. However, a major limitation exists in the direct application of IGFBP2 to the wound site without a carrier system, as it is prone to rapid dissipation or degradation [52-54]. In contrast, IRA-NFPs are specifically designed to provide structural support while functioning as a controlled release system for IGFBP2, enabling a sustained and prolonged healing process rather than a single application. Furthermore, IRA-NFPs demonstrate potential to effectively promote regeneration even in patients with large tympanic membrane perforations. By integrating structural guidance with IGFBP2 delivery, this approach may enhance the efficiency of healing in severe cases where conventional treatments often result in suboptimal outcomes. While surgical method required high cost, anesthesia risks, microsurgical skills of surgeon, this method has no risk of anesthesia, low cost, and easy application for patients. In the context of human subjects, patch maintenance is comparatively more straightforward than in animal models, as certain patches have the tendency to detach from the TMs over the course of 8 weeks. In histological investigation, TMs regenerated using AF-w/IGFBP2 exhibited comparable thickness to normal TMs, while TMs healed using RF-w/IGFBP2 displayed greater thickness than that of normal TMs. The effective revitalization of TMs could potentially be impacted by the radially aligned nanostructure of AF-w/IGFBP2.

Table 2
Healing rate of chronic TM perforations by IGFBP2-releasing nanofibrous patches.

week	0	1	2	3	4	5	6	7	8
SH	0/33 (0 %)	0/33 (0 %)	0/33 (0 %)	0/33 (0 %)	0/33 (0 %)	0/33 (0 %)	0/33 (0 %)	3/33 (9.1 %)	4/33 (12.1 %)
RF-w/IGFBP2	0/26 (0 %)	3/26 (11.5 %)	5/26 (19.2 %)	5/26 (19.2 %)	5/26 (19.2 %)	5/26 (19.2 %)	5/26 (19.2 %)	5/26 (19.2 %)	6/26 (23.1 %)
AF-w/IGFBP2	0/37 (0 %)	7/37 (18.9 %)	7/37 (18.9 %)	8/37 (21.6 %)	8/37 (21.6 %)	8/37 (21.6 %)	8/37 (21.6 %)	8/37 (21.6 %)	10/37 (27.0 %)

It has been demonstrated that electrospun aligned fibers significantly influence cell orientation and function, particularly in soft tissues [55-58]. This property suggests that electrospun aligned nanofibers have the potential to improve cell orientation in TM and serve as suitable scaffolds for TM reconstruction. However, while the structural benefits of aligned nanofibers are well-documented, the interaction between these scaffolds and latent stem cells in the context of TM regeneration remains to be fully elucidated. Further mechanism studies are needed to investigate how aligned nanofibers influence the activation, proliferation, and differentiation of latent stem cells *in vivo*. Understanding these cellular mechanisms is crucial for optimizing scaffold design and maximizing its regenerative potential. Such studies could reveal how the nanostructure influences the behavior of resident stem cells and potentially enhances their contribution to TM regeneration. Additionally, our previous study has significantly identified latent stem cells, particularly present in proximity to the TM perforations, which may serve as potential regulators of regeneration [41]. Therefore, exploring the interplay between the nanofibers, latent stem cells, and IGFBP2 could provide valuable insights into the synergistic effects observed in TM regeneration. Considering that the thickness of the TM intimately correlates with the transmission of sound vibrations, the radially aligned nanostructure could serve as a promising foundation for the restoration of chronic TM perforations. Our preliminary results suggest that the combined use of IGFBP2 and radially aligned nanostructure may have a synergistic effect for chronic TM perforation. This synergy likely stems from the nanostructure's ability to guide cell orientation and role of IGFBP2 in stem cell activation, though the exact mechanisms require further investigation. By integrating these approaches, we may be able to develop more effective strategies for TM regeneration, potentially improving outcomes for patients with chronic TM perforations.

5. Conclusion

The objective of this study was to produce nanofibrous patches capable of releasing growth factors, aiming to address chronic perforations of the TM. Their radial alignment and their potential for growth factor release were verified via a characterization analysis. In the initial experiment, functional regeneration of the TM was prompted by radially aligned patterns in conjunction with IGFBP2, as opposed to randomly aligned patterns. This approach holds promise as an effective strategy for the restoration of chronic TM perforations and, in the long run, for the healing of chronic otitis media.

Declaration of competing interest

The authors declare that they have no known competing financial interests or personal relationships that could have appeared to influence the work reported in this paper.

CRediT authorship contribution statement

Juo Lee: Writing – review & editing, Writing – original draft, Methodology, Formal analysis. **Sangbae Park:** Writing – review & editing, Writing – original draft, Methodology, Formal analysis. **Beomyong Shin:** Writing – original draft, Methodology, Formal analysis, Conceptualization. **Yeon Ju Kim:** Visualization, Methodology, Data curation. **Sungmin Lee:** Visualization, Methodology, Formal analysis. **Jungsil Kim:** Writing – review & editing, Methodology, Formal analysis. **Kyoung-Je Jang:** Investigation. **Oak-Sung Choo:** Investigation. **Jangho Kim:** Investigation. **Hoon Seonwoo:** Writing – review & editing, Writing – original draft, Supervision, Resources, Project administration, Investigation, Funding acquisition, Conceptualization. **Jong Hoon Chung:** Supervision, Resources, Project administration, Investigation. **Yun-Hoon Choung:** Supervision, Resources, Project administration, Funding acquisition.

Acknowledgment

All authors deeply appreciate Iksong Byun of the Department of Convergent Biosystems Engineering at Sunchon National University for assistance with in vitro experiments, and Jinhyun Kim of the Department of Biosystems Engineering at Seoul National University for contributions to patch fabrication and reference verification. This research was supported by a grant of the Korea Health Technology R&D Project through the Korea Health Industry Development Institute (KHIDI), funded by the Ministry of Health & Welfare, Republic of Korea (Grant No. HI15C-0968-000015, 10%), Basic Science Research Program (NRF-2019R1I1A3A01064005, 10%) and "Regional Innovation Strategy (RIS)" (2021RIS-002, 10%) through the National Research Foundation of Korea (NRF) funded by the Ministry of Education, and Innovative Human Resource Development for Local Intellectualization program through the Institute of Information & Communications Technology Planning & Evaluation(IITP) grant funded by the Korea government (MSIT) (IITP-2024-RS-2020-II201489, 70%).

Data availability

All data are available from the corresponding author upon reasonable request.

Supplementary materials

Supplementary material associated with this article can be found, in the online version, at doi:10.1016/j.actbio.2024.09.019.

References

[1] A.J. Lee, R.K. Jackler, B.M. Kato, N.M. Scott, Repair of chronic tympanic membrane perforations using epidermal growth factor: progress toward clinical application, Otol. Neurotol. 15 (1) (1994) 10–18.
[2] P. Caye-Thomasen, T.R. Nielsen, M. Tos, Bilateral myringoplasty in chronic otitis media, Laryngoscope 117 (5) (2007) 903–906.
[3] C.H. Jang, Y.B. Cho, M. Yeo, H. Lee, E.J. Min, B.H. Lee, G.H. Kim, Regeneration of chronic tympanic membrane perforation using 3D collagen with topical umbilical cord serum, Int. J. Biol. Macromol. 62 (2013) 232–240.
[4] P. Hong, M. Bance, P.F. Gratzer, Repair of tympanic membrane perforation using novel adjuvant therapies: a contemporary review of experimental and tissue engineering studies, Int. J. Pediatr. Otorhinolaryngol. 77 (1) (2013) 3–12.
[5] Q. Zhang, Z. Lou, Impact of basic fibroblast growth factor on healing of tympanic membrane perforations due to direct penetrating trauma: a prospective non-blinded/controlled study, Clin. Otolaryngol. 37 (6) (2012) 446–451.
[6] V.W. Wong, G.C. Gurtner, M.T. Longaker, in: Wound healing: a Paradigm For Regeneration, Mayo Clinic Proceedings, Elsevier, 2013, pp. 1022–1031.
[7] S.J. Choi, J.H. Kim, O.S. Choo, Y.H. Choung, Efficient treatment of chronic tympanic membrane perforations in animal models by chitosan patch scaffolds, Tissue Eng. Regen. Med. 8 (2) (2011) 141–150.
[8] S.W. Yeo, S.-W. Kim, B.-D. Suh, S.-H. Cho, Effects of platelet-derived growth factor-AA on the healing process of tympanic membrane perforation, Am. J. Otolaryngol. 21 (3) (2000) 153–160.
[9] J.T. Vrabec, M.K. Schwaber, J.M. Davidson, M.A. Clymer, Evaluation of basic fibroblast growth factor in tympanic membrane repair, Laryngoscope 104 (9) (1994) 1059–1064.
[10] A.Y. Wang, Y. Shen, L.J. Liew, J.T. Wang, M. von Unge, M.D. Atlas, R.J. Dilley, Searching for a rat model of chronic tympanic membrane perforation: healing delayed by mitomycin C/dexamethasone but not paper implantation or iterative myringotomy, Int. J. Pediatr. Otorhinolaryngol. 79 (8) (2015) 1240–1247.
[11] D.E. Weber, M.T. Semaan, J.K. Wasman, R. Beane, L.J. Bonassar, C.A. Megerian, Tissue-engineered calcium alginate patches in the repair of chronic chinchilla tympanic membrane perforations, Laryngoscope 116 (5) (2006) 700–704.
[12] H. Seonwoo, B. Shin, K.J. Jang, M. Lee, O.S. Choo, S.B. Park, Y.C. Kim, M.J. Choi, J. Kim, P. Garg, Epidermal growth factor–releasing radially aligned electrospun nanofibrous patches for the regeneration of chronic tympanic membrane perforations, Adv. Healthc. Mater. 8 (2) (2019) 1801160.
[13] H.A. Ramsay, E.J. Heikkonen, P.K. Laurila, Effect of epidermal growth factor on tympanic membranes with chronic perforations: a clinical trial, Otolaryngol.—Head Neck Surg. 113(4) (1995) 375–379.

[14] J.R. Ramalho, R.F. Bento, Healing of subacute tympanic membrane perforations in chinchillas treated with epidermal growth factor and pentoxifylline, Otol. Neurotol. 27 (5) (2006) 720–727.
[15] P.L. Santa Maria, K. Weierich, S. Kim, Y.P. Yang, Heparin binding epidermal growth factor-like growth factor heals chronic tympanic membrane perforations with advantage over fibroblast growth factor 2 and epidermal growth factor in an animal model, Otol. Neurotol. 36 (7) (2015) 1279–1283.
[16] D.R. Clemmons, Role of IGF binding proteins in regulating metabolism, Trends Endocrinol. Metab. 27 (6) (2016) 375–391.
[17] J.H. Kim, S.J. Choi, J.-S. Park, K.T. Lim, P.-H. Choung, S.W. Kim, J.B. Lee, J.H. Chung, Y.-H. Choung, Tympanic membrane regeneration using a water-soluble chitosan patch, Tissue Eng. Part A 16 (1) (2010) 225–232.
[18] C.-Y. Kuo, E. Wilson, A. Fuson, N. Gandhi, R. Monfaredi, A. Jenkins, M. Romero, M. Santoro, J.P. Fisher, K. Cleary, Repair of tympanic membrane perforations with customized bioprinted ear grafts using chinchilla models, Tissue Eng. Part A 24 (5–6) (2018) 527–535.
[19] Y. Shen, S.L. Redmond, B.M. Teh, S. Yan, Y. Wang, M.D. Atlas, R.J. Dilley, M. Zheng, R.J. Marano, Tympanic membrane repair using silk fibroin and acellular collagen scaffolds, Laryngoscope 123 (8) (2013) 1976–1982.
[20] A. Tamae, S. Komune, Clinical study of transcanal closure of tympanic membrane perforations using a collagen sponge, J. Laryngol. Otol. 129 (S2) (2015) S21–S26.
[21] B. Azimi, M. Milazzo, S. Danti, Cellulose-based fibrous materials from bacteria to repair tympanic membrane perforations, Front. Bioeng. Biotechnol. 9 (2021) 669863.
[22] H. Seonwoo, S.W. Kim, B. Shin, K.-J. Jang, M. Lee, O.-S. Choo, M.-J. Choi, J. Kim, K.-T. Lim, J.H. Jang, Latent stem cell-stimulating therapy for regeneration of chronic tympanic membrane perforations using IGFBP2-releasing chitosan patch scaffolds, J. Biomater. Appl. 34 (2) (2019) 198–207.
[23] H. Seonwoo, S.W. Kim, J. Kim, T. Chunjie, K.T. Lim, Y.J. Kim, S. Pandey, P.-H. Choung, Y.-H. Choung, J.H. Chung, Regeneration of chronic tympanic membrane perforation using an EGF-releasing chitosan patch, Tissue Eng. Part A 19 (17–18) (2013) 2097–2107.
[24] J. Xie, X. Li, J. Lipner, C.N. Manning, A.G. Schwartz, S. Thomopoulos, Y. Xia, Aligned-to-random" nanofiber scaffolds for mimicking the structure of the tendon-to-bone insertion site, Nanoscale 2 (6) (2010) 923–926.
[25] J. Kim, H.N. Kim, K.-T. Lim, Y. Kim, H. Seonwoo, S.H. Park, H.J. Lim, D.-H. Kim, K.-Y. Suh, P.-H. Choung, Designing nanotopographical density of extracellular matrix for controlled morphology and function of human mesenchymal stem cells, Sci. Rep. 3 (1) (2013) 3552.
[26] B. Azimi, A. Rasti, A. Fusco, T. Macchi, C. Ricci, M.A. Hosseinifard, L. Guazzelli, G. Donnarumma, R. Bagherzadeh, M. Latifi, Bacterial cellulose electrospun fiber mesh coated with chitin nanofibrils for eardrum repair, Tissue Eng. Part A 30 (7–8) (2024) 340–356.
[27] J. Xie, M.R. MacEwan, W.Z. Ray, W. Liu, D.Y. Siewe, Y. Xia, Radially aligned, electrospun nanofibers as dural substitutes for wound closure and tissue regeneration applications, ACS Nano 4 (9) (2010) 5027–5036.
[28] D. Duscher, J. Barrera, V.W. Wong, Z.N. Maan, A.J. Whittam, M. Januszyk, G.C. Gurtner, Stem cells in wound healing: the future of regenerative medicine? A mini-review, Gerontology 62 (2) (2016) 216–225.
[29] V.W. Wong, B. Levi, J. Rajadas, M.T. Longaker, G.C. Gurtner, Stem cell niches for skin regeneration, Int. J. Biomater. 2012 (1) (2012) 926059.
[30] S. Goncalves, E. Bas, B.J. Goldstein, S. Angeli, Effects of cell-based therapy for treating tympanic membrane perforations in mice, Otolaryngol.–Head Neck Surg. 154(6) (2016) 1106–1114.
[31] H.R. Hofer, R.S. Tuan, Secreted trophic factors of mesenchymal stem cells support neurovascular and musculoskeletal therapies, Stem Cell Res. Ther. 7 (2016) 1–14.
[32] C.H. Jang, S. Ahn, J.W. Lee, B.H. Lee, H. Lee, G. Kim, Mesenchymal stem cell-laden hybrid scaffold for regenerating subacute tympanic membrane perforation, Mater. Sci. Eng.: C 72 (2017) 456–463.
[33] K.C. Rustad, V.W. Wong, M. Sorkin, J.P. Glotzbach, M.R. Major, J. Rajadas, M.T. Longaker, G.C. Gurtner, Enhancement of mesenchymal stem cell angiogenic capacity and stemness by a biomimetic hydrogel scaffold, Biomaterials 33 (1) (2012) 80–90.
[34] G. Ren, L. Zhang, X. Zhao, G. Xu, Y. Zhang, A.I. Roberts, R.C. Zhao, Y. Shi, Mesenchymal stem cell-mediated immunosuppression occurs via concerted action of chemokines and nitric oxide, Cell Stem Cell 2 (2) (2008) 141–150.
[35] D. Duscher, E. Neofytou, V.W. Wong, Z.N. Maan, R.C. Rennert, M. Inayathullah, M. Januszyk, M. Rodrigues, A.V. Malkovskiy, A.J. Whitmore, Transdermal deferoxamine prevents pressure-induced diabetic ulcers, Proc. Natl. Acad. Sci. 112 (1) (2015) 94–99.
[36] S. Loges, T. Schmidt, P. Carmeliet, Antimyeloangiogenic" therapy for cancer by inhibiting PlGF, Clin. Cancer Res. 15 (11) (2009) 3648–3653.
[37] S. Perveen, H. Patel, A. Arif, S. Younis, C.N. Codipilly, M. Ahmed, Role of EC–SOD overexpression in preserving pulmonary angiogenesis inhibited by oxidative stress, PLoS One 7 (12) (2012) e51945.
[38] E.I. Chang, S.A. Loh, D.J. Ceradini, E.I. Chang, S.-e. Lin, N. Bastidas, S. Aarabi, D.A. Chan, M.L. Freedman, A.J. Giaccia, Age decreases endothelial progenitor cell recruitment through decreases in hypoxia-inducible factor 1α stabilization during ischemia, Circulation 116 (24) (2007) 2818–2829.
[39] P.L. Santa Maria, M.D. Atlas, R. Ghassemifar, Chronic tympanic membrane perforation: a better animal model is needed, Wound Repair Regener. 15 (4) (2007) 450–458.
[40] V. Russo, W. Azar, S. Yau, M. Sabin, G. Werther, IGFBP-2: the dark horse in metabolism and cancer, Cytokine Growth Factor Rev. 26 (3) (2015) 329–346.
[41] S.W. Kim, J. Kim, H. Seonwoo, K.-J. Jang, Y.J. Kim, H.J. Lim, K.-T. Lim, C. Tian, J.H. Chung, Y.-H. Choung, Latent progenitor cells as potential regulators for tympanic membrane regeneration, Sci. Rep. 5 (1) (2015) 11542.
[42] G.W. Radebaugh, J.L. Murtha, T.N. Julian, J.N. Bondi, Methods for evaluating the puncture and shear properties of pharmaceutical polymeric films, Int. J. Pharm. 45 (1–2) (1988) 39–46.
[43] D. Kai, M.P. Prabhakaran, G. Jin, S. Ramakrishna, Guided orientation of cardiomyocytes on electrospun aligned nanofibers for cardiac tissue engineering, J. Biomed. Mater. Res. Part B: Appl. Biomater. 98 (2) (2011) 379–386.
[44] J.Y. Chung, J.P. Youngblood, C.M. Stafford, Anisotropic wetting on tunable micro-wrinkled surfaces, Soft. Matter. 3 (9) (2007) 1163–1169.
[45] H. Kunhiraman, L. McSwain, S.W. Shahab, T.R. Gershon, T.J. MacDonald, A.M. Kenney, IGFBP2 promotes proliferation and cell migration through STAT3 signaling in Sonic hedgehog medulloblastoma, Acta Neuropathol. Commun. 11 (1) (2023) 62.
[46] B. Mroczkowski, R. Ball, Epidermal growth factor: biology and properties of its gene and protein precursor, in: Growth Factors, Differentiation Factors, and Cytokines, Springer, 1990, pp. 18–30.
[47] V. Perez-Puyana, P. Wieringa, A. Guerrero, A. Romero, L. Moroni, Macro) Molecular imprinting of proteins on PCL electrospun scaffolds, ACS Appl. Mater. Interfaces 13 (25) (2021) 29293–29302.
[48] A. Lancuški, F. Bossard, S. Fort, Carbohydrate-decorated PCL fibers for specific protein adhesion, Biomacromolecules 14 (6) (2013) 1877–1884.
[49] G. Volandri, F. Di Puccio, P. Forte, C. Carmignani, Biomechanics of the tympanic membrane, J. Biomech. 44 (7) (2011) 1219–1236.
[50] K. Onal, S. Arslanoglu, M. Songu, U. Demiray, I. Demirpehlivan, Functional results of temporalis fascia *versus* cartilage tympanoplasty in patients with bilateral chronic otitis media, J. Laryngol. Otol. 126 (1) (2012) 22–25.
[51] J. Ha, H. Kim, J.H. Jang, H.Y. Park, Y.-H. Choung, Transtympanic soft tissue tympanoplasty can replace conventional techniques elevating tympanic membranes, Eur. Arch. Oto-Rhino-Laryngol. 279 (12) (2022) 5639–5645.
[52] X. Yao, B.M. Teh, H. Li, Y. Hu, J. Huang, C. Lv, S. Bu, M. Zheng, Y. Shen, Acellular collagen scaffold with basic fibroblast growth factor for repair of traumatic tympanic membrane perforation in a rat model, Otolaryngol.–Head Neck Surg. 164(2) (2021) 381–390.
[53] L. Benington, Development and characterisation of an optimised basic fibroblast growth factor (FGF-2) formulation for the repair of chronic tympanic membrane perforations, (2020).
[54] D. Shahal, S. Goncalves, S.I. Angeli, Mesenchymal stem cells for treatment of delayed-healing tympanic membrane perforations using hyaluronate-based laminas as a delivery system: an animal model with histopathologic study, Otol. Neurotol. 43 (4) (2022) e497–e506.
[55] L. Ghasemi-Mobarakeh, M.P. Prabhakaran, M. Morshed, M.H. Nasr-Esfahani, S. Ramakrishna, Electrical stimulation of nerve cells using conductive nanofibrous scaffolds for nerve tissue engineering, Tissue Eng. Part A 15 (11) (2009) 3605–3619.
[56] M.P. Prabhakaran, J.R. Venugopal, S. Ramakrishna, Mesenchymal stem cell differentiation to neuronal cells on electrospun nanofibrous substrates for nerve tissue engineering, Biomaterials 30 (28) (2009) 4996–5003.
[57] Z. Chen, P. Wang, B. Wei, X. Mo, F. Cui, Electrospun collagen–chitosan nanofiber: a biomimetic extracellular matrix for endothelial cell and smooth muscle cell, Acta Biomater. 6 (2) (2010) 372–382.
[58] Z. Ma, W. He, T. Yong, S. Ramakrishna, Grafting of gelatin on electrospun poly (caprolactone) nanofibers to improve endothelial cell spreading and proliferation and to control cell orientation, Tissue Eng. 11 (7–8) (2005) 1149–1158.